catalysts

Article

Iron-Modified Functional Biochar Activates Peroxydisulfate for Efficient Degradation of Organic Pollutants

Weijie Chen [1,2], Bingbing Zhang [1], Hao Pu [1], Zhao Yang [1], Yixue Qin [1], Mingze An [1], Chengtao Gao [1], Kang Mao [3,*], Sheng Wang [1,*], Bing Xue [1] and Caiyuan Sun [4]

[1] Guizhou Material Industrial Technology Institute, Guiyang 550014, China; chenweijie5031@163.com (W.C.); puhao7799@163.com (H.P.); amz921810@163.com (M.A.)
[2] College of Resources and Environmental Engineering, Guizhou University, Guiyang 550025, China
[3] State Key Laboratory of Environmental Geochemistry, Institute of Geochemistry, Chinese Academy of Sciences, Guiyang 550081, China
[4] Chutian Liangjiang Environment Co., Ltd., Guiyang 550000, China; scy1633528@126.com
* Correspondence: maokang@mail.gyig.ac.cn (K.M.); willa_wangsheng@126.com (S.W.)

Abstract: Tetracycline (TC) contamination in wastewater presents a significant global environmental challenge, with conventional water treatment methods often proving ineffective at eliminating antibiotic pollutants. As a result, there is an urgent need for cost-effective and efficient remediation technologies. In this study, we utilized the abundant and low-cost *Eichhornia crassipes* as a precursor to prepare sulfuric acid-modified functional biochar (SC-Fe) through a two-step pyrolysis process. This SC-Fe was then employed to activate peroxydisulfate (PDS) for the removal of TC from wastewater. The structural and physicochemical properties of SC-Fe were extensively characterized, and its efficiency in activating PDS for TC degradation was evaluated. The results demonstrated that the SC-Fe/PDS system effectively removed 99.36% of TC within 60 min under optimal conditions (0.3 g/L SC-Fe, 5 mM PDS, initial pH 7.09, and 25 °C). The outstanding removal efficiency can be attributed to the high specific surface area, large porosity, and defect-rich structure of SC-Fe. Furthermore, during the TC removal process, the SC-Fe/PDS system generated $SO_4^{\bullet-}$, •OH, and $^1O_2$, with $SO_4\bullet^-$ and •OH acting as the primary reactive species. The high catalytic efficiency and low consumption of the SC-Fe/PDS system present a promising strategy for effective wastewater treatment.

Keywords: functional biochar; peroxydisulfate activation; tetracycline removal; Eichhornia crassipes-derived material; two-step pyrolysis method; resource utilization

check for updates

Academic Editor: John Vakros

Received: 10 March 2025
Revised: 4 May 2025
Accepted: 4 May 2025
Published: 8 May 2025

Citation: Chen, W.; Zhang, B.; Pu, H.; Yang, Z.; Qin, Y.; An, M.; Gao, C.; Mao, K.; Wang, S.; Xue, B.; et al. Iron-Modified Functional Biochar Activates Peroxydisulfate for Efficient Degradation of Organic Pollutants. *Catalysts* **2025**, *15*, 462. https://doi.org/10.3390/catal15050462

Copyright: © 2025 by the authors. Licensee MDPI, Basel, Switzerland. This article is an open access article distributed under the terms and conditions of the Creative Commons Attribution (CC BY) license (https://creativecommons.org/licenses/by/4.0/).

1. Introduction

Tetracycline (TC), a broad-spectrum antibiotic valued for its potent bacteriostatic activity and cost-effectiveness, has been extensively employed in human medicine, livestock production, and agricultural practices [1]. According to recent statistical data, China ranks among the global leaders in TC production, consumption, and exportation, with annual exports exceeding 13,400 metric tons [2]. The pervasive discharge of TC-contaminated wastewater has raised substantial concerns regarding its ecotoxicological impacts and potential human health risks through environmental accumulation, emerging as a pressing environmental challenge requiring immediate remediation strategies [3]. Peroxysulfate (PS)-based advanced oxidation processes (AOPs) have gained increasing scientific attention as promising solutions for organic pollutant degradation. This preference stems from PS's favorable characteristics, including exceptional chemical stability, superior oxidation capacity (E^0 = 1.82–2.01 V), operational efficiency, and environmental compatibility [4,5]. While

both peroxymonosulfate (PMS) and peroxydisulfate (PDS) are categorized as PS derivatives, comparative analyses reveal that PDS demonstrates a higher redox potential (2.01 V vs. 1.82 V for PMS), endowing it with enhanced oxidative capabilities for contaminant degradation [6]. The enhanced stability of PDS arises from its robust peroxy bonds (O-O bond energy: 140 kJ/mol), which exhibit remarkable resistance to spontaneous cleavage compared to PMS counterparts [7]. This inherent stability necessitates external activation through catalytic processes to generate reactive oxygen species (ROS), highlighting the importance of developing efficient activation methodologies.

Biochar has emerged as a sustainable catalytic platform for PDS activation due to its high specific surface area, abundant ion exchange sites, and hierarchical porosity. However, pristine biochar typically exhibits suboptimal catalytic performance due to intrinsic limitations, including insufficient active site density, impaired structural integrity under prolonged oxidative stress, and limited functional group diversity [8]. Conventional chemical impregnation methods, although widely used for surface modification, tend to cause the aggregation of nanoparticles and secondary contamination through the leaching of synthetic precursors (e.g., HNO_3 or KOH residues), which can reduce the catalytic efficiency by 40–60% [9]. Conversely, one study demonstrated that by using iron-modified biocarbon, not only can the problems of chemical aggregation and environmental hazards be solved but PDS can also be effectively activated to remove tetracycline [10].

Eichhornia crassipes is widely used in the restoration of aquatic environments due to its excellent Fe^{2+} adsorption capacity. However, the effective resource utilization of this plant after remediation remains a significant challenge. Therefore, in this study, *Eichhornia crassipes* was utilized as the raw material, and a plant enrichment method combined with a two-step pyrolysis process was employed to prepare ferrous sulfate-modified functional biochar (SC-Fe). This biochar was then used to activate PDS for the degradation of TC pollutants in the water environment, exploring a novel approach for the resource utilization of adsorption plants. The morphology and structure of SC-Fe were characterized in detail, and relevant system parameters were optimized. The effects of various factors, including different systems, SC-Fe dosage, PDS dosage, initial pH values, and coexisting anions, on tetracycline removal were investigated. Additionally, the radical mechanisms involved in the tetracycline removal process were analyzed, providing new reference pathways for the removal of tetracycline antibiotics.

2. Results and Discussion

2.1. Biomass Characterization Results

SC-Fe exhibits a significantly altered surface morphology characterized by distinct groove-like channels, numerous interconnected pores, and a highly disordered and rough texture. These prominent features result from the secondary pyrolysis and strong alkaline etching effect induced by KOH activation, which markedly enhance the porosity and surface irregularity of the material. The formation of a hierarchical pore structure—comprising both micropores and mesopores—not only increases the specific surface area but also facilitates the rapid diffusion and penetration of target pollutants and oxidants, thereby improving the overall reaction kinetics. Moreover, the rough surface of SC-Fe contains numerous exposed edges, fractured lattice regions, and surface cracks, indicating a high density of structural defects. These defects are widely regarded as catalytically active sites capable of effectively adsorbing and activating oxidants such as persulfate, leading to the generation of reactive species (e.g., $SO_4^{\bullet -}$ and •OH) for the efficient degradation of tetracycline. Together, these characteristics contribute to the outstanding catalytic activity and recyclability of SC-Fe in environmental remediation applications [11] (Figure 1).

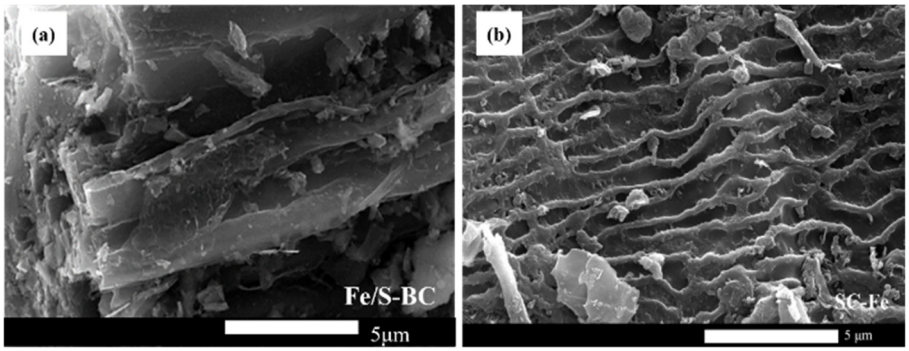


Figure 1. SEM images of (**a**) Fe/S-BC and (**b**) SC-Fe.

The N_2 adsorption–desorption isotherms, pore size distribution curves, and pore size histograms of Fe/S-BC and SC-Fe are presented in Figure 2a–d. According to the IUPAC classification, both samples exhibit reversible Type IV isotherms with H3-type hysteresis loops, which are typically associated with slit-shaped mesopores formed by the aggregation of plate-like particles. Notably, the hysteresis loops for SC-Fe do not close at high relative pressures (P/P_0 approaching 1), indicating incomplete desorption. These observations suggest that SC-Fe has a complex mesoporous structure with significant pore connectivity and potential structural flexibility, which are important considerations for its application in adsorption and catalysis processes. The specific surface area, average pore diameter, and total pore volume of Fe/S-BC and SC-Fe are summarized in Table 1. The specific surface area of SC-Fe (480 m^2/g) is 34 times higher than that of Fe/S-BC (14 m^2/g), and the total pore volume of SC-Fe (0.280 cc/g) is 10 times greater than that of Fe/S-BC (0.028 cc/g). This indicates that the secondary pyrolysis of Fe/S-BC mixed with KOH in a specific ratio effectively enhances the specific surface area and total porosity. Consequently, the high activity of SC-Fe can be attributed to its larger specific surface area and porous structure.

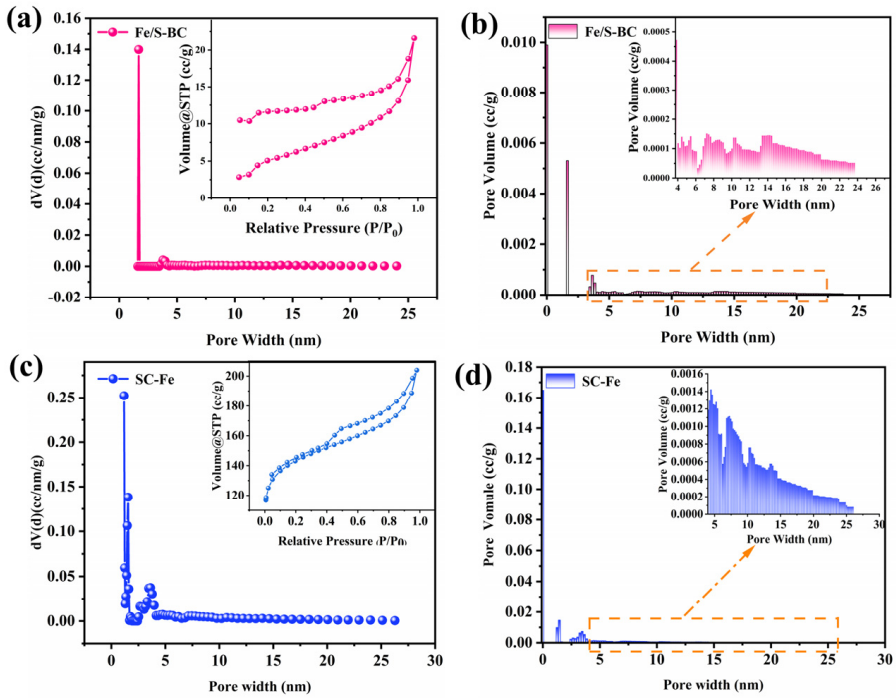


Figure 2. (**a**) N_2 adsorption–desorption isotherm and pore size distribution curves of Fe/S-BC, (**b**) pore size distribution histograms of Fe/S-BC, (**c**) N_2 adsorption–desorption isotherms and pore size distribution curves of SC-Fe, and (**d**) pore size distribution histograms of SC-Fe.

Table 1. Specific surface area, average pore size, and total pore volume of Fe/S-BC and SC-Fe.

Sample	S_{BET} (m^2 g^{-1})	Pore Size (nm)	Pore Volume (cc/g)
Fe/S-BC	14	1.766	0.028
SC-Fe	480	1.178	0.280

S_{BET} in the table is the specific surface area of Fe/S-BC and SC-Fe.

X-ray diffraction (XRD) patterns were used to characterize the crystal structures of all the synthesized catalysts. The XRD spectra of Fe/S-BC and SC-Fe are shown in Figure 3a,b, respectively. As seen in the figures, broad diffraction peaks corresponding to amorphous carbon (002) and graphite carbon (100) appear in 2θ ranges of 20–30° and 40–50°, respectively [12]. However, the broad diffraction peaks in SC-Fe are more pronounced, indicating that the enrichment of Fe and S, combined with secondary pyrolysis under high-temperature conditions, promotes the formation of the amorphous carbon structure of SC-Fe, providing more defect sites.

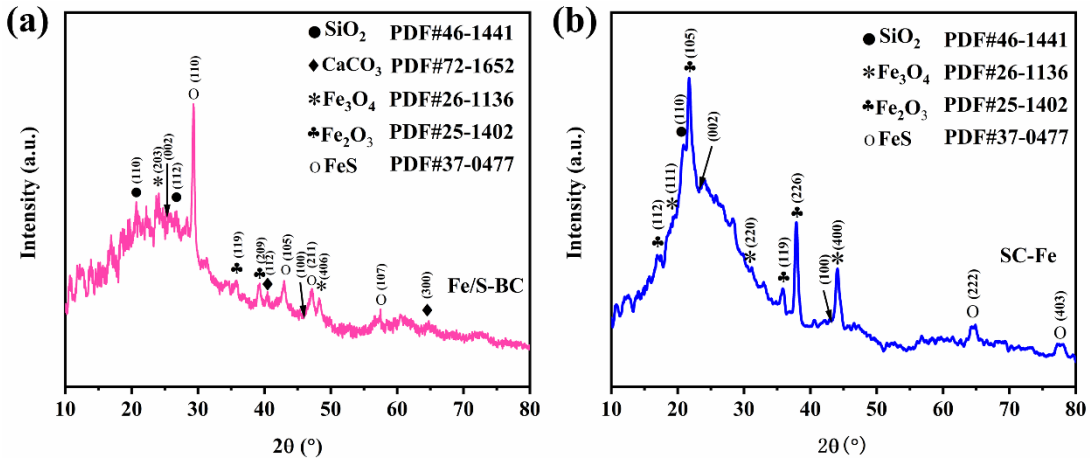


Figure 3. (**a**) XRD spectra of Fe/S-BC; (**b**) XRD spectra of SC-Fe.

In both Fe/S-BC and SC-Fe, Fe exists in the forms of Fe_3O_4, Fe_2O_3, and FeS. Specifically, the peaks at 2θ values of 44.76°, 20.69°, 35.69°, 37.31°, 64.38°, and 77.77° in SC-Fe correspond to the (400) peak of Fe_3O_4; the (105), (119), and (226) peaks of Fe_2O_3; and the (222) and (403) peaks of FeS. Compared to Fe/S-BC, SC-Fe exhibits better crystalline structures, which can be attributed to the enhanced formation of Fe_3O_4, Fe_2O_3, and FeS after KOH treatment and the secondary pyrolysis of Fe/S-BC [13].

Raman spectroscopy was further employed to analyze the carbon configurations of Fe/S-BC and SC-Fe, as shown in Figure 4a–c. The G_2 peak at 1580 cm^{-1} to 1588 cm^{-1} is associated with the stretching vibration of carbon in a fully sp^2 hybridized state (sp^2-C), reflecting the level of carbon graphitization. The D_1 peak at 1341 cm^{-1} can be attributed to the defective graphite lattice (sp^2 disordered C) [14]. The ID_1/IG_2 ratio serves as a crucial indicator of the disorder and defect levels in the carbon material. The Raman parameters are summarized in Table 2. The ID_1/IG_2 ratios for Fe/S-BC and SC-Fe are 1.49 and 1.86, respectively. At the same time, the area ratio of the S_3 peak in the Raman spectrum reflects the degree of disordered carbon and structural defects in the material. The S_3 ratio in the SC-Fe sample has increased significantly, indicating that its surface contains more structural defects, which helps to provide additional active sites for the adsorption and activation of PDS. At the same time, the defective structure is also conducive to the generation and migration of free radicals, thereby effectively improving the degradation efficiency of TC. The increase in amorphous carbon indicates that the secondary pyrolysis of Fe/S-BC, rich

in Fe and S, induces a higher amount of amorphous carbon, promoting the formation of more defect sites and providing additional active sites for PDS activation.

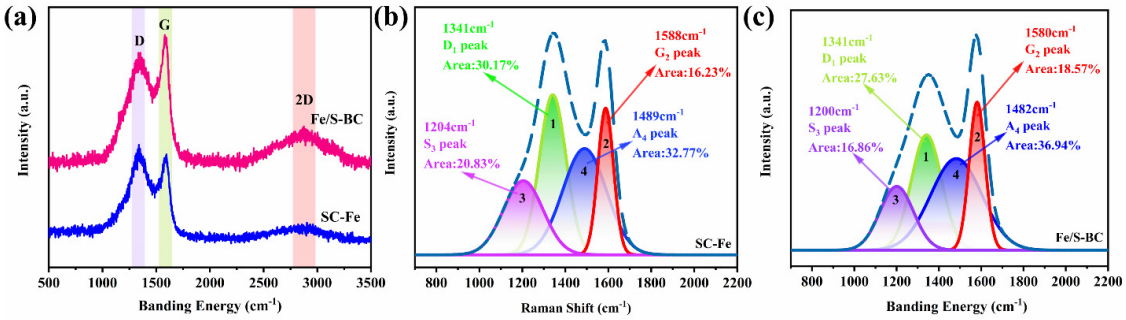


Figure 4. Raman spectra of (**a**) Fe/S-BC and SC-Fe, (**b**) Raman peak spectra of Fe/S-BC, and (**c**) Raman peak spectra of SC-Fe.

Table 2. Raman parameters of Fe/S-BC and SC-Fe.

Catalysts	D_1 (%)	S_3 (%)	A_4 (%)	G_2 (%)	ID_1/IG_2
Fe/S-BC	27.63%	16.86%	36.94%	18.57%	1.49
SC-Fe	30.17%	20.83%	32.77%	16.23%	1.86

D_1 (%) is the percentage of the subpeak area of the D peak located at ~1341 cm^{-1}; S_3 (%) is the percentage of the area of the third subpeak in the split-peak fit; A_4 (%) is the percentage of the area of the subpeak associated with amorphous carbon; G_2 (%) is the percentage of the area of the subpeak of the G peak located at ~1580 cm^{-1}; and ID/IG is the ratio of the intensity of the D_1 peak to that of the intensity ratio of the G_2 peak.

X-ray photoelectron spectroscopy (XPS) is widely used to investigate the elemental composition, electronic structure, and chemical states of material surfaces. XPS was employed to determine the elemental composition and chemical states of Fe/S-BC and SC-Fe, as shown in Figure 5. Both Fe/S-BC and SC-Fe contain C 1s, O 1s, N 1s, S 2p, and Fe 2p elements. Notably, SC-Fe shows significantly higher intensities at 164.1 eV (corresponding to thionyl sulfur, -C-S-C), 398.1 eV (attributed to pyridinic nitrogen), and 710.8 eV (associated with Fe^{2+}) compared to Fe/S-BC. The formation of these chemical species can provide additional potential active sites for PDS activation. These results suggest that the higher activity of SC-Fe may be due to the presence of thionyl sulfur (-C-S-C), pyridinic nitrogen, and Fe^{2+} [15,16].

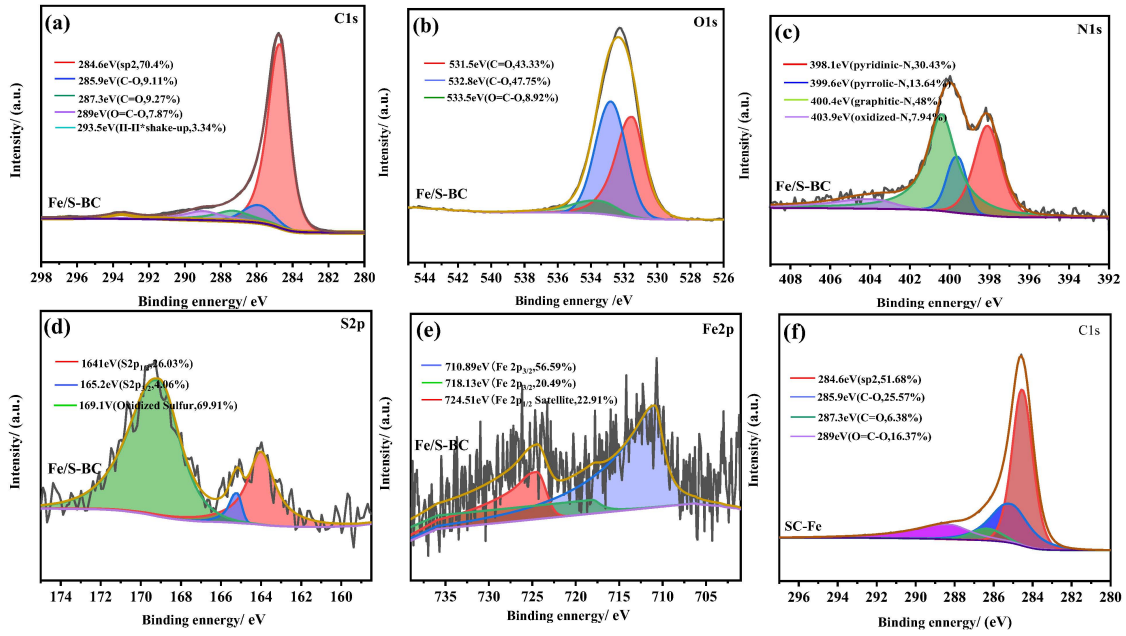


Figure 5. *Cont.*

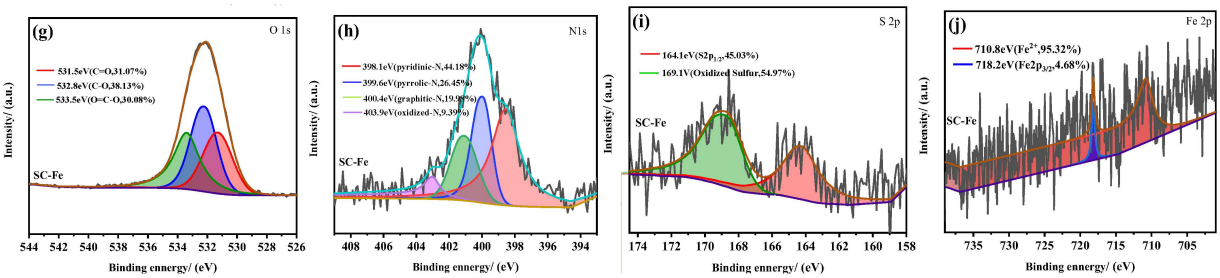


Figure 5. XPS fine spectra of Fe/S-BC (**a**) C 1s, (**b**) O 1s, (**c**) N 1s, (**d**) S 2p, and (**e**) Fe 2p; XPS fine spectra of SC-Fe (**f**) C 1s, (**g**) O 1s, (**h**) N 1s, (**i**) S 2p, and (**j**) Fe 2p.

2.2. Optimization of System Parameters for TC Removal Experiment

To investigate the effectiveness of SC-Fe-activated PDS for the removal of TC from wastewater. The effects of different variables (different systems, SC-Fe dosages, PDS dosages, initial pH, and co-existing anions) on the removal of TC by the system were investigated, and the active radicals involved in the removal of TC by the system were identified.

As shown in Figure 6a, the PDS system, Fe/S-BC/PDS system, and SC-Fe/PDS system were established to evaluate the removal efficiency for TC. The removal efficiencies for TC in the three systems were 22.4%, 59.0%, and 99.4%, respectively. These results suggest that PDS alone has limited effectiveness in removing TC, while the addition of Fe/S-BC or SC-Fe significantly enhances the removal efficiency. Among them, SC-Fe exhibits the highest TC removal rate, making it the selected activator for further study in the system. To enhance the removal of TC in the system, the effect of SC-Fe dosage on TC removal efficiency was investigated, as shown in Figure 6b. In the figure, it can be observed that as the SC-Fe dosage increases from 0.1 g/L to 0.3 g/L, the TC removal efficiency in the system steadily increases, reaching 78.7%, 90.9%, and 99.4%. However, when the SC-Fe dosage is further increased from 0.3 g/L to 0.5 g/L, there is negligible improvement in TC removal. This is because excessive SC-Fe can consume the generated $SO_4\bullet^-$ in the system, hindering TC removal [17]. Therefore, 0.3 g/L was selected as the optimal SC-Fe dosage for the system in subsequent studies.

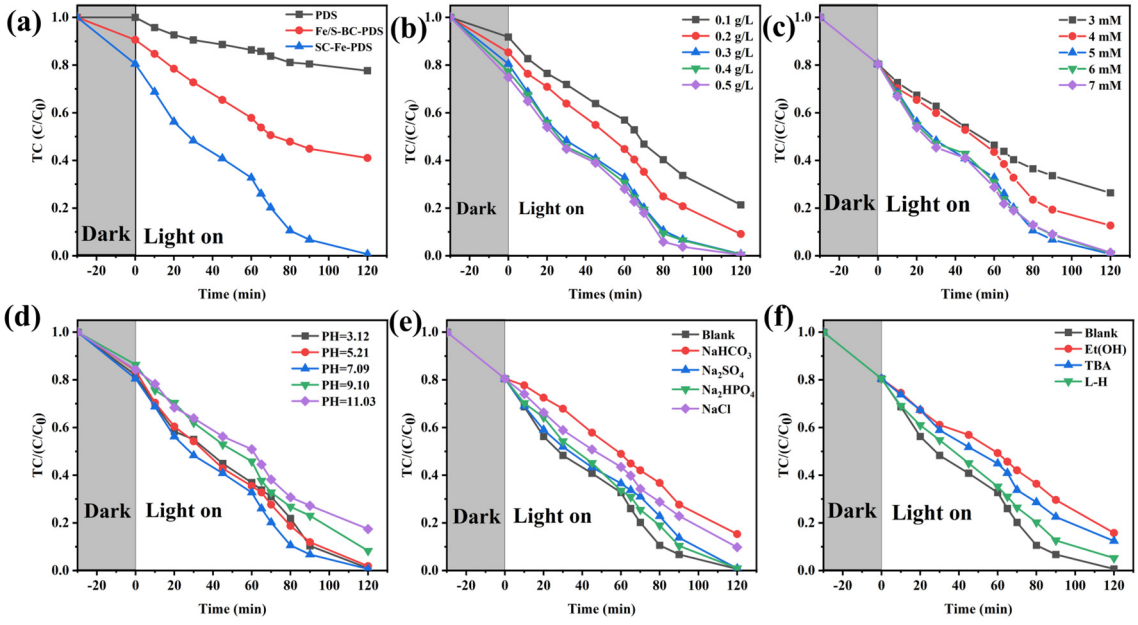


Figure 6. (**a**) Performance of TC removal in different systems (experimental conditions: catalyst: 0.3 g/L; PDS: 5 mM; pH: 7. 09; T: 25 °C). (**b**) Effect of SC-Fe dosage on TC removal in the system

(experimental conditions: PDS:5 mM; pH: 7.09; T: 25 °C). (**c**) Effect of PDS dosage on TC removal in the system (experimental conditions: catalyst: 0.3 g/L; pH: 7.09; T: 25 °C). (**d**) Effect of initial pH on TC removal (experimental conditions: catalyst: 0.3 g/L; PDS:5 mM; T: 25 °C). (**e**) Influence of coexisting anions on TC removal in the SC-Fe/PDS system. (**f**) Effects of Et(OH), TBA, and L-H on TC removal in the SC-Fe/PDS system (experimental conditions: catalyst: 0.3 g/L; PDS:5 mM; pH: 7.09; T: 25 °C).

The effect of different PDS dosages on TC removal efficiency in the system was investigated, as shown in Figure 6c. As the PDS dosage increased from 3 mM to 5 mM, the TC removal rate improved from 73.6% to 99.4% within 60 min. This enhancement is likely due to the increased generation of highly oxidative free radicals as the PDS dosage increases. However, when the PDS dosage was further increased to 7 mM, there was no further improvement in TC removal; instead, the removal rates decreased to 99.1% and 98.6%. This decline may be attributed to the saturation of the PDS activation sites, competition for adsorption sites between PDS and TC on the surface of SC-Fe, and the self-quenching effects of excess PDS, as shown in Equations (2) and (3) [18,19]. Therefore, 5 mM was selected as the optimal PDS dosage for the system.

$$SO_4^{\bullet -} + SO_4^{\bullet -} \rightarrow S_2O_8^{2-} \quad (1)$$

$$SO_4^{\bullet -} + S_2O_8^{2-} \rightarrow S_2O_8^{\bullet -} + SO_4^{2-} \quad (2)$$

The initial pH is one of the most critical factors in the persulfate advanced oxidation process. Therefore, the effect of initial pH (ranging from 3.12 to 11.03) on TC removal efficiency was investigated, as shown in Figure 6d. In the figure, it can be observed that when the initial pH of the solution is between 3.12 and 7.09, the TC removal rates are 99.0%, 98.1%, and 99.4%, with minimal impact on TC removal, indicating that the pH range for this system is broad. However, when the initial pH of the solution is 9.10 and 11.03, the TC removal rate is significantly inhibited. This may be due to the formation of iron hydroxide precipitates on the surface of SC-Fe under strong alkaline conditions, which hinder the formation of active sites [20]. Another possible reason is the self-consumption of the generated $SO_4\bullet^-$ and •OH radicals under alkaline conditions, as shown in Equations (4) and (5) [21,22]. Additionally, under different initial pH conditions, the forms of SC-Fe and TC in the reaction solution may change, resulting in electrostatic repulsion that prevents TC from adsorbing onto the SC-Fe surface, thus hindering TC removal [23].

$$SO_4^{\bullet -} + OH^- \rightarrow SO_4^{2-} + \bullet OH \quad (3)$$

$$\bullet OH + \bullet OH \rightarrow H_2O_2 \quad (4)$$

Inorganic anions are widely present in natural water bodies and may either positively or negatively affect the system during the reaction process. The impact of coexisting anions on TC removal efficiency in the SC-Fe/PDS system was investigated. As shown in Figure 6e, the addition of SO_4^{2-} and HPO_4^{2-} had a minimal effect on TC removal, with removal rates decreasing by only 0.2% and 0.3%, respectively. However, the addition of HCO_3^- and Cl^- significantly inhibited TC removal. This inhibition is likely due to the reaction between Cl^- and the $SO_4\bullet^-$ radicals generated in the system (Equation (6)), forming the less oxidative Cl• radical. Cl^- can also react with •OH (Equations (7) and (8)) to produce weaker oxidative species such as OH^- and $Cl_2\bullet^-$. As the reaction progresses, the generated Cl^- and Cl• further lead to the formation of low-oxidative $Cl_2\bullet^-$ (Equation (9)), which hinders TC removal due to the generation of less effective radicals [24,25]. The addition of HCO_3^- also reacts with $SO_4\bullet^-$ and •OH (Equations (10) and (11)) to form low-activity radicals, further suppressing the reaction. Another possible explanation for the inhibition

is that the addition of HCO_3^- elevates the solution pH, which, in turn, reduces TC removal, resembling the decreased removal observed under alkaline conditions [26,27].

$$SO_4^{\bullet-} + Cl^- \rightarrow SO_4^{2-} + Cl^{\bullet} \quad (5)$$

$$Cl^- + \bullet OH \rightarrow ClOH^{\bullet-} \quad (6)$$

$$ClOH^{\bullet-} + Cl^- \rightarrow Cl_2^{\bullet-} + OH^- \quad (7)$$

$$Cl^- + Cl^{\bullet} \rightarrow Cl_2^{\bullet-} \quad (8)$$

$$HCO_3^- + SO_4^{\bullet-} \rightarrow SO_4^{2-} + HCO_3^{\bullet} \quad (9)$$

$$HCO_3^- + \bullet OH \rightarrow H_2O + CO_3^{\bullet-} \quad (10)$$

To identify the primary reactive radicals involved in the TC removal process, ethanol (EtOH), tert-butyl alcohol (TBA), and L-histidine (L-H) were employed as scavengers for $SO_4\bullet^-$ and •OH, •OH, and $^1O_2$, respectively. As shown in Figure 6f, the addition of these three scavengers led to a significant reduction in TC removal, with removal rates of 84.2%, 87.6%, and 94.8%, respectively. These findings suggest that the key active radicals responsible for TC removal in the system are $SO_4\bullet^-$, •OH, and $^1O_2$, with $SO_4\bullet^-$ and •OH playing the predominant roles.

2.3. Reusability of SC-Fe

Figure 7 depicts the TC removal efficiency of the SC-Fe/PDS system over five consecutive cycles. As shown, the removal efficiency gradually decreased with each successive cycle, which may be due to the accumulation of residual TC on the SC-Fe surface or the leaching of iron from SC-Fe, both of which likely reduced the number of available active sites. The TC removal rates after five cycles were 99.4%, 99.0%, 86.1%, 81.2%, and 76.3%. Despite the observed decline in efficiency, the SC-Fe/PDS system retained a TC removal rate of 76.3% after five cycles, highlighting the exceptional stability and reusability of SC-Fe. These results underscore its potential as a highly promising catalyst for TC removal.

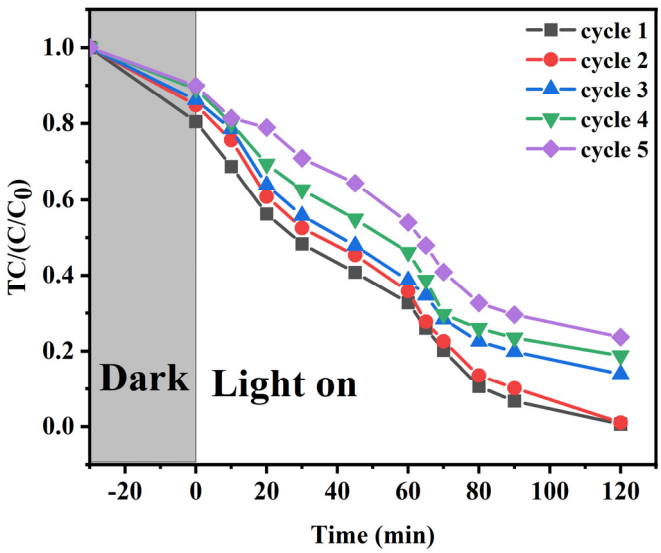


Figure 7. Removal effect on TC during SC-Fe recycling (experimental conditions: catalyst: 0.3 g/L; PDS:5 mM; pH: 7.09; T: 25 °C).

3. Materials and Methods

3.1. Raw Materials

Eichhornia crassipes was collected from a natural lake in Shantou, Guangdong. Ferrous sulfate ($FeSO_4 \cdot 7H_2O$), hydrochloric acid (HCl), and sodium thiosulfate ($Na_2S_2O_3$) were purchased from Sinopharm Chemical Reagent Co., Ltd., Shanghai, China. Sodium persulfate ($Na_2S_2O_8$, 99%), tetracycline (TC), and sodium bicarbonate ($NaHCO_3$, ≥99.5%) were obtained from Macklin Biochemical Co., Ltd., Shanghai, China. Absolute ethanol (EtOH, 99.7%) (AR), tert-butanol (TBA), and L-histidine (L-H, ≥99%) were purchased from Aladdin, Shanghai, China. Sodium sulfate (Na_2SO_4) (AR) and sodium chloride (NaCl) (AR) were sourced from Chongqing Chuandong Chemical (Group, Chongqing City, China) Co., Ltd., while hydrochloric acid (HCl) and sodium hydroxide (NaOH) (AR) were obtained from Chengdu Kelong Chemical Reagent Factory. Disodium hydrogen phosphate ($Na_2HPO_4 \cdot 12H_2O$, ≥99%) was purchased from Tianjin Damao Chemical Reagent Factory. All chemicals were of analytical grade and were used without further purification. Unless otherwise specified, all solutions were prepared with deionized water. In this case, *Eichhornia crassipes* was used as a precursor of biochar; $FeSO_4 \cdot 7H_2O$ provided Fe^{2+} ions for plant enrichment; KOH was used as a chemical activator to enhance the porosity of biochar; HCl was used to remove residual impurities and unreacted KOH from the surface of biochar; $Na_2S_2O_8$ and PDS were used as oxidizers to generate sulfate radicals; TC mimicked antibiotic contaminants as target contaminants; $Na_2S_2O_3$ quenched residual radicals in the reaction system; HCl and NaOH were used to regulate the initial pH of the reaction solution; NaCl, Na_2SO_4, $NaHCO_3$, and Na_2HPO_4 were used to mimic common inorganic anions found in natural waters; and EtOH and TBA were used as trapping agents for SO_4^{2-} and -OH, respectively. L-H trapped single linear oxygen ($^1O_2$); deionized water reduced ionic interference and ensured solution purity.

3.2. Instruments and Equipment

A scanning electron microscope (SEM, Quanta FEG250) was obtained from FEI Company, USA. The specific testing conditions are as follows: resolution of 0.8 nm at 1 kV, accelerating voltage ranging from 1 kV to 20 kV, and magnification of 100–300,000×. The specific surface area and porosity analyzer (BET, Nova-1000e) was obtained from Quantachrome Corporation, USA. The specific testing conditions were as follows: the adsorbed gas was nitrogen, the testing temperature was −196 °C, vacuum degassing was performed at 150 °C, and the degassing time was 12 h. A Raman spectrometer was also used (Raman, LabRAM HR Odyssey). The specific testing conditions were as follows: Raman shift: 0~4000, laser wavelength: 514 nm, spectral resolution: 4 cm^{-1}, and exposure time:10 s. An X-ray diffractometer (XRD, X'Pert PRO) was obtained from PANalytical, the Netherlands. The specific testing conditions were as follows: tube current was 40 mA, tube voltage was 40 kV, incident wavelength was 0.15418 nm, X-ray output source was 3 kW with a Cu target as the radiation source, scanning range was 5–90°, and the scanning mode was continuous mode. An X-ray photoelectron spectrometer (XPS, Thermo Scientific K-Alpha) was obtained from Nicolet, USA. The specific testing conditions were as follows: Al Kα radiation was used as the light source, with a tube current of 10 mA and a testing tube voltage of 15 kV. The binding energy of the sample was calibrated using the C 1s peak (284.8 eV).

3.3. Preparation of Modified Biochar

Eichhornia crassipes samples were collected from a lake, thoroughly rinsed with deionized water, and then transferred to a simulated Fe^{2+}-contaminated aquatic environment containing 200 mg/L of ferrous sulfate heptahydrate ($FeSO_4 \cdot 7H_2O$) for a 34-day cultivation

period. The collected plants were thoroughly rinsed with deionized water, cut into small pieces, and dried in a forced-air oven at 80 °C for 48 h. The dried samples were then placed in a tube furnace, heated to 600 °C at a rate of 5 °C/min under a nitrogen flow of 80 mm Hg/min, and held at this temperature for 2 h. Following the heating process, the system was allowed to cool naturally to room temperature, resulting in the formation of Fe/S-BC. The prepared Fe/S-BC was ground, sieved, and mixed with KOH at a 1:4 mass ratio and then transferred to a 100 mL beaker and combined with 30 mL of deionized water. The beaker was sealed with plastic wrap, allowing the Fe/S-BC and KOH mixture to soak for 1 h. Subsequently, the mixture was heated in a water bath at 100 °C to evaporate the water until a paste-like consistency was achieved, at which point, heating was stopped. The paste was then transferred to a tube furnace, heated to 350 °C at a rate of 5 °C/min, held for 1 h, and further heated to 800 °C at the same rate, where it was held for 1 h before being naturally cooled to room temperature. The resulting sample was repeatedly washed with 10 wt% HCl, ethanol, and deionized water and then dried in an oven at 120 °C for 24 h to obtain the final product, referred to as SC-Fe.

3.4. Experiment on Modified Biochar Activating PDS for TC Removal

The experiments were conducted in 50 mL amber centrifuge tubes with a working volume of 40 mL, and all reactions were performed in a digital thermostatic water-bath oscillator at 25 °C and 200 rpm. Tetracycline (TC) at an initial concentration of 10 mg/L was used as the model pollutant. Various experimental conditions were investigated, including different systems (PDS, Fe/S-BC/PDS, and SC-Fe/PDS), catalyst dosages, PDS concentrations, initial pH values, and the presence of co-existing anions. To ensure adsorption–desorption equilibrium, Fe/S-BC or SC-Fe was first thoroughly mixed with the TC solution and stirred in the dark for 30 min (corresponding to an interval of *x*-axis less than zero). After the dark pre-equilibration phase, the reaction was initiated by adding PDS, and the system was then exposed to light to trigger the photocatalytic degradation process. At designated time intervals (0, 10, 20, 30, 45, 60, 65, 70, 80, 90, and 120 min), a 0.5 mL aliquot was withdrawn from the reaction system, immediately quenched with 0.2 M of sodium thiosulfate, filtered through a 0.45 μm polyethersulfone (PES) membrane, and collected in EP tubes. The residual TC concentration was analyzed immediately using a UV–vis spectrophotometer at its maximum absorption wavelength of 357 nm. The removal efficiency was calculated using Equation (1):

$$\text{Removal rate}(\%) = \frac{C_0 - C_t}{C_0} \times 100\% \quad (11)$$

In the above equation, C_0 and C_t are the initial concentration of organic pollutants and the concentration at a certain time, respectively.

4. Conclusions

In this study, a sustainable and efficient TC removal strategy was demonstrated by combining Fe-modified biochar with an advanced oxidation process. The synthesized SC-Fe exhibited excellent physicochemical properties, including a high specific surface area (480.15 m^2/g), an abundant pore structure, and a defect-rich carbon framework, which provided sufficient active sites for PDS activation. Under optimal conditions (SC-Fe dosage of 0.3 g/L, PDS dosage of 5 mM, initial pH of the solution 7.09, and temperature of 25 °C), the system achieved a TC removal efficiency of 99.36% within 60 min. Mechanistic studies showed that SO_4^- and -OH played a dominant role in the degradation process, while $^1O_2$ played a secondary role. The system maintained stable performance over a wide pH range (3.12–11.03) but was significantly inhibited in alkaline environments or in the presence of Cl^- and HCO_{-3} due to free radical scavenging. In addition, SC-Fe

showed excellent reusability, maintaining 76.34% efficiency after five cycles. This work emphasizes the dual advantages of resource recovery and environmental remediation using hyperaccumulating plants, providing a scalable and eco-friendly solution for antibiotic-contaminated wastewater treatment.

Author Contributions: Methodology, H.P., M.A., and C.G.; Software, Z.Y. and B.X.; Formal analysis, B.Z.; Investigation, Y.Q. and K.M.; Data curation, S.W. and C.S.; Writing—review and editing, W.C. All authors have read and agreed to the published version of the manuscript.

Funding: Guizhou Science and Technology Support Program—[2022] General219; Guizhou Province Science and Technology Talent Project—QCC[2025]005; Guizhou Provincial Basic Research Program (Natural Science)—QKHJC-ZK [2023] YB158; Guizhou Science and Technology Support Program—[2024] General048; Guizhou Science and Technology Achievement Program—[2023] General739.

Data Availability Statement: The original contributions presented in this study are included in the article. Further inquiries can be directed to the corresponding author(s).

Conflicts of Interest: Author Caiyuan Sun was employed by the company Chutian Liangjiang Environment Co., Ltd. The remaining authors declare that the research was conducted in the absence of any commercial or financial relationships that could be construed as a potential conflict of interest.

References

1. Liu, Y.; Kong, J.; Yuan, J.; Zhao, W.; Zhu, X.; Sun, C.; Xie, J. Enhanced photocatalytic activity over flower-like sphere $Ag/Ag_2CO_3/BiVO_4$ plasmonic heterojunction photocatalyst for tetracycline degradation. *Chem. Eng. J.* **2018**, *331*, 242–254. [CrossRef]
2. Zhang, T.; Yang, Y.; Li, W.; Zhou, Y.; Wu, L.; Cheng, Z. Adsorption of tetracycline by alkali-modified biochar. *J. Yichun Coll.* **2022**, *44*, 6–12+47.
3. Yuan, H.; Li, C.; Wei, Y.; Zhu, Y.; Zuo, W.; Tong, H. FeOCl Composite peanut shell-derived biochar Activated by persulfate for degradation of tetracycline. *Chem. Technol. Dev.* **2023**, *52*, 7–10.
4. Ouyang, D.; Chen, Y.; Yan, J.; Qian, L.; Han, L.; Chen, M. Activation mechanism of peroxymonosulfate by biochar for catalytic degradation of 1,4-dioxane: Important role of biochar defect structures. *Chem. Eng. J.* **2019**, *370*, 614–624. [CrossRef]
5. Li, F.; Duan, F.; Ji, W.; Gui, X. Biochar-activated persulfate for organic contaminants removal: Efficiency, mechanisms and influencing factors. *Ecotoxicol. Environ. Saf.* **2020**, *198*, 110653. [CrossRef]
6. Xiao, S.; Cheng, M.; Zhong, H.; Liu, Z.; Liu, Y.; Yang, X.; Liang, Q. Iron-mediated activation of persulfate and peroxymonosulfate in both homogeneous and heterogeneous ways: A review. *Chem. Eng. J.* **2020**, *384*, 123265. [CrossRef]
7. Wacławek, S.; Lutze, H.V.; Grübel, K.; Padil, V.V.; Černík, M.; Dionysiou, D.D. Chemistry of persulfates in water and wastewater treatment: A review. *Chem. Eng. J.* **2017**, *330*, 44–62. [CrossRef]
8. Huang, Q.; Song, S.; Chen, Z.; Hu, B.; Chen, J.; Wang, X. Biochar-based materials and their applications in removal of organic contaminants from wastewater: State-of-the-art review. *Biochar* **2019**, *1*, 45–73. [CrossRef]
9. Yu, F.; Tian, F.; Zou, H.; Ye, Z.; Peng, C.; Huang, J.; Zheng, Y.; Zhang, Y.; Yang, Y.; Wei, X.; et al. ZnO/biochar nanocomposites via solvent free ball milling for enhanced adsorption and photocatalytic degradation of methylene blue. *J. Hazard. Mater.* **2021**, *415*, 125511. [CrossRef]
10. Xu, R.; Li, M.; Zhang, Q. Collaborative optimization for the performance of ZnO/biochar composites on persulfate activation through plant enrichment-pyrolysis method. *Chem. Eng. J.* **2022**, *429*, 132294. [CrossRef]
11. Hou, X.; Dong, H.; Li, Y.; Xiao, J.; Dong, Q.; Xiang, S.; Chu, D. Activation of persulfate by graphene/biochar composites for phenol degradation: Performance and nonradical dominated reaction mechanism. *J. Environ. Chem. Eng.* **2023**, *11*, 109348. [CrossRef]
12. Zhong, S.; Pan, J.; Tian, K.; Qin, J.; Qing, T.; Zhang, J. Efficient degradation of p-chlorophenol by N,S-co-doped biochar activated perxymonosulfate. *Process Saf. Environ. Prot.* **2023**, *169*, 437–446. [CrossRef]
13. Sierra, I.; Iriarte-Velasco, U.; Ayastuy, J.L.; Aguayo, A.T. Production of magnetic sewage sludge biochar: Investigation of the activation mechanism and effect of the activating agent and temperature. *Biomass Convers. Biorefinery* **2022**, *13*, 17101–17118. [CrossRef]
14. Shimodaira, N.; Masui, A. Raman spectroscopic investigations of activated carbon materials. *J. Appl. Phys.* **2002**, *92*, 902–909. [CrossRef]
15. Li, C.; Xu, B.; Jin, M.; Chen, L.; Yi, G.; Chen, L.; Wu, Y.; Zhang, Y.; Xing, B. Sulfur and nitrogen co-doped biochar activated persulfate to degrade phenolic wastewater: Changes in impedance. *J. Mol. Struct.* **2023**, *1294*, 136344. [CrossRef]

16. Huang, R.; Feng, T.; Wu, S.; Zhang, X.; Fan, Z.; Yu, Q.; Chen, Y.; Chen, T. In-situ synthesis of magnetic iron-chitosan-derived biochar as an efficient persulfate activator for phenol degradation. *Environ. Res.* **2023**, *234*, 116604. [CrossRef]
17. Liu, G.; Zhang, Y.; Yu, H.; Jin, R.; Zhou, J. Acceleration of goethite-catalyzed Fenton-like oxidation of ofloxacin by biochar. *J. Hazard. Mater.* **2020**, *397*, 122783. [CrossRef] [PubMed]
18. Introduction. In *Encyclopedia of Condensed Matter Physics*, 2nd ed.; Chakraborty, T., Ed.; Academic Press: Oxford, UK, 2024; pp. ix–xvii.
19. Hussain, I.; Li, M.; Zhang, Y.; Li, Y.; Huang, S.; Du, X.; Liu, G.; Hayat, W.; Anwar, N. Insights into the mechanism of persulfate activation with nZVI/BC nanocomposite for the degradation of nonylphenol. *Chem. Eng. J.* **2017**, *311*, 163–172. [CrossRef]
20. Xi, M.; Cui, K.; Cui, M.; Ding, Y.; Guo, Z.; Chen, Y.; Li, C.; Li, X. Enhanced norfloxacin degradation by iron and nitrogen co-doped biochar: Revealing the radical and nonradical co-dominant mechanism of persulfate activation. *Chem. Eng. J.* **2021**, *420*, 129902. [CrossRef]
21. Stuglik, Z.; Pawełzagórski, Z. Pulse radiolysis of neutral iron (II) solutions: Oxidation of ferrous ions by OH radicals. *Radiat. Phys. Chem.* **1981**, *17*, 229–233. [CrossRef]
22. Chen, K.F.; Kao, C.M.; Wu, L.C.; Surampalli, R.Y.; Liang, S.H. Methyl tert-butyl ether (MTBE) degradation by ferrous ion-activated persulfate oxidation: Feasibility and kinetics studies. *Water Environ. Res.* **2009**, *81*, 687–694. [CrossRef]
23. Zhang, Y.; Shi, J.; Xu, Z.; Chen, Y.; Song, D. Degradation of tetracycline in a schorl/H_2O_2 system: Proposed mechanism and intermediates. *Chemosphere* **2018**, *202*, 661–668. [CrossRef] [PubMed]
24. Huang, Q.; Chen, C.; Zhao, X.; Bu, X.; Liao, X.; Fan, H.; Gao, W.; Hu, H.; Zhang, Y.; Huang, Z. Malachite green degradation by persulfate activation with $CuFe_2O_4$@biochar composite: Efficiency, stability and mechanism. *J. Environ. Chem. Eng.* **2021**, *9*, 105800. [CrossRef]
25. Zhou, Z.; Liu, X.; Sun, K.; Lin, C.; Ma, J.; He, M.; Ouyang, W. Persulfate-based advanced oxidation processes (AOPs) for organic-contaminated soil remediation: A review. *Chem. Eng. J.* **2019**, *372*, 836–851. [CrossRef]
26. Fu, H.; Zhao, P.; Xu, S.; Cheng, G.; Li, Z.; Li, Y.; Li, K.; Ma, S. Fabrication of Fe_3O_4 and graphitized porous biochar composites for activating peroxymonosulfate to degrade p-hydroxybenzoic acid: Insights on the mechanism. *Chem. Eng. J.* **2019**, *375*, 121980. [CrossRef]
27. Song, H.; Li, Q.; Ye, Y.; Pan, F.; Zhang, D.; Xia, D. Degradation of cephalexin by persulfate activated with magnetic loofah biochar: Performance and mechanism. *Sep. Purif. Technol.* **2021**, *272*, 118971. [CrossRef]

Disclaimer/Publisher's Note: The statements, opinions and data contained in all publications are solely those of the individual author(s) and contributor(s) and not of MDPI and/or the editor(s). MDPI and/or the editor(s) disclaim responsibility for any injury to people or property resulting from any ideas, methods, instructions or products referred to in the content.